Supporting Information

Atomic Ru Immobilized on Porous h-BN through Simple Vacuum Filtration for Highly Active and Selective CO_2 Methanation

Mengmeng Fan, Juan D. Jimenez, Sharmila N. Shirodkar, Jingjie Wu*, Shuang ming Chen, Li Song, Michael M. Royko, Junjie Zhang, Hua Guo, Jiewu Cui, Kuichang Zuo, Weipeng Wang, Chenhao Zhang, Fanshu Yuan, Robert Vajtai, Jieshu Qian, Jiazhi Yang, Boris I. Yakobson, James M. Tour, Jochen Lauterbach*, Dongping Sun*, Pulickel M. Ajayan*

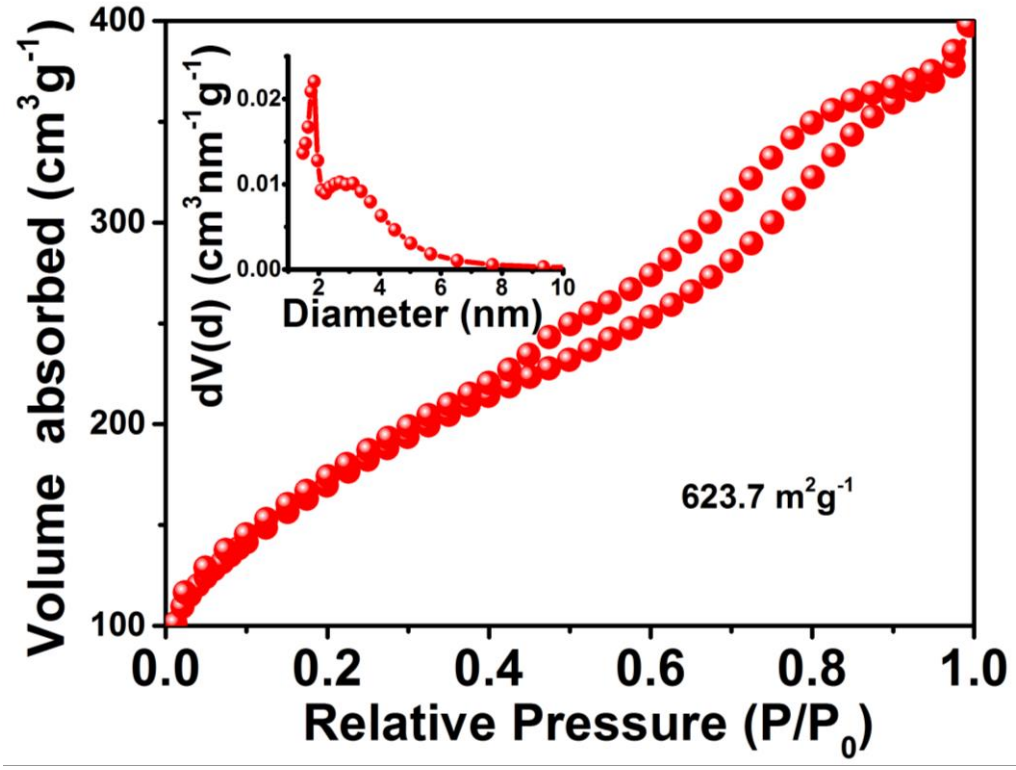

Figure S1. N_2 adsorption-desorption isotherms inset, the pore diameter distribution curves of pBN.

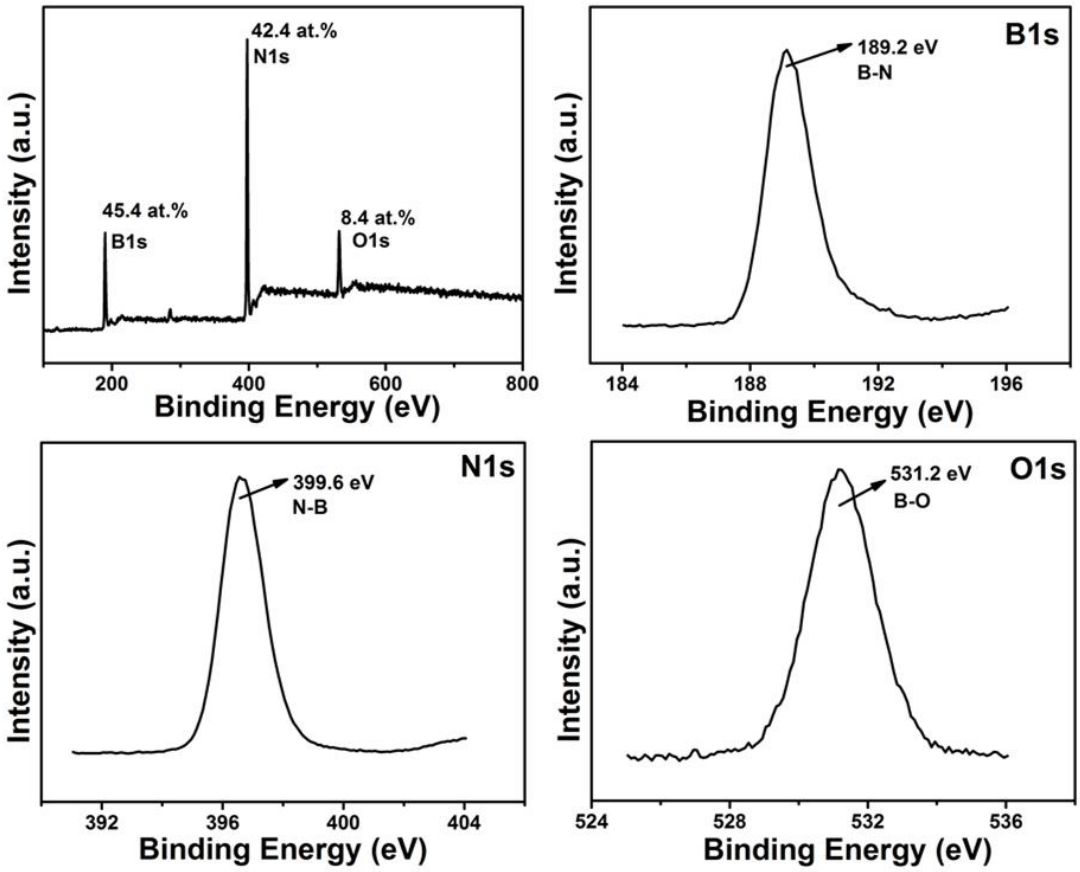

Figure S2. The XPS characterization of pBN: survey spectrum and B1s, N1s and O1s.

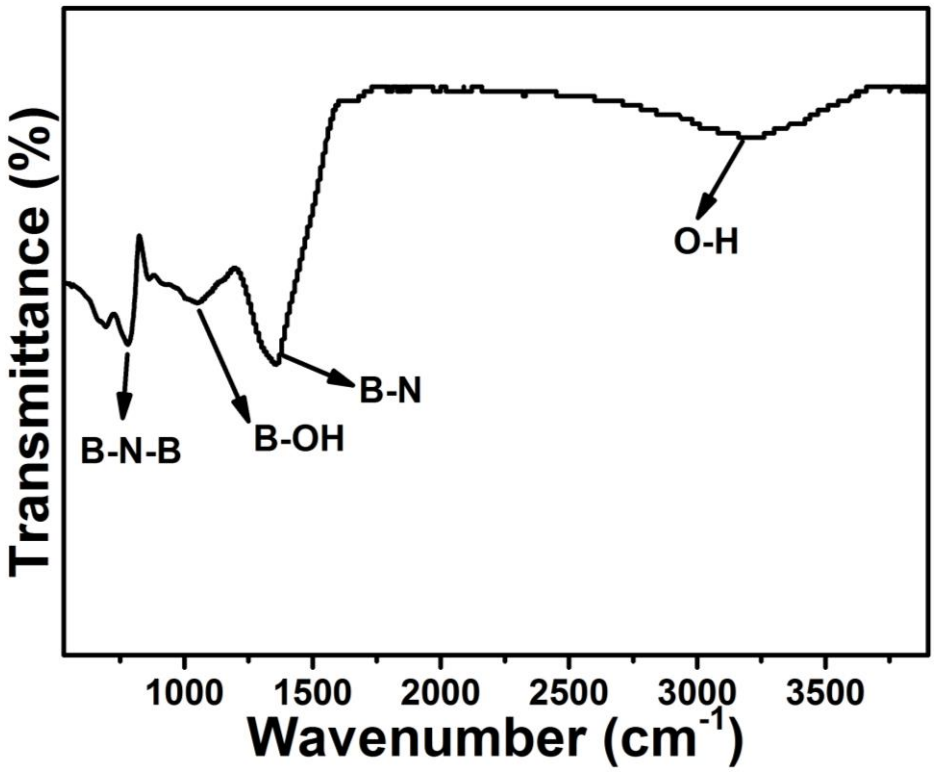

Figure S3. the FT-IR spectrum of pBN.

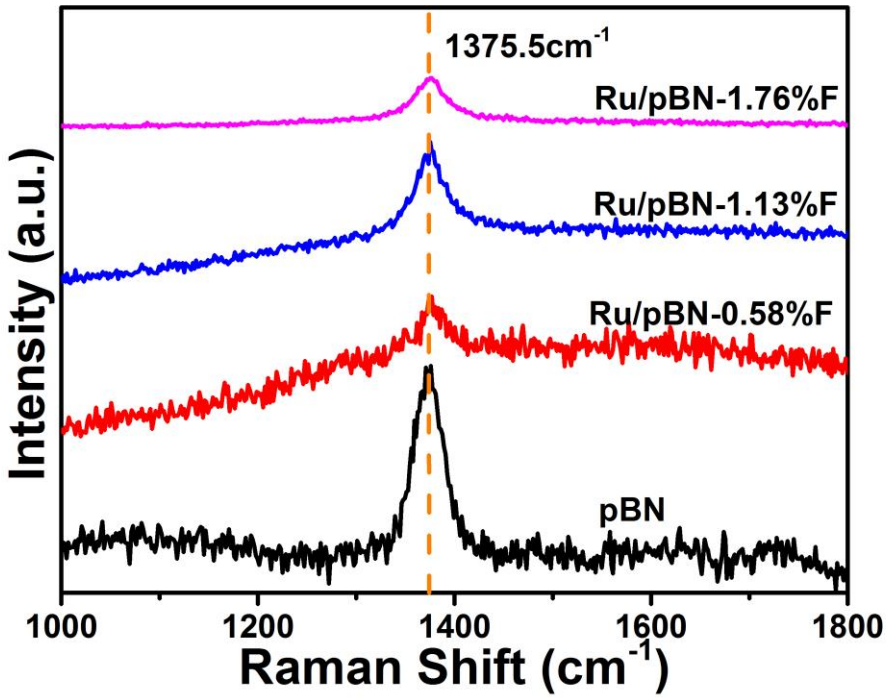

Figure S4. Raman spectras of pBN and Ru/pBN-*x*F samples.

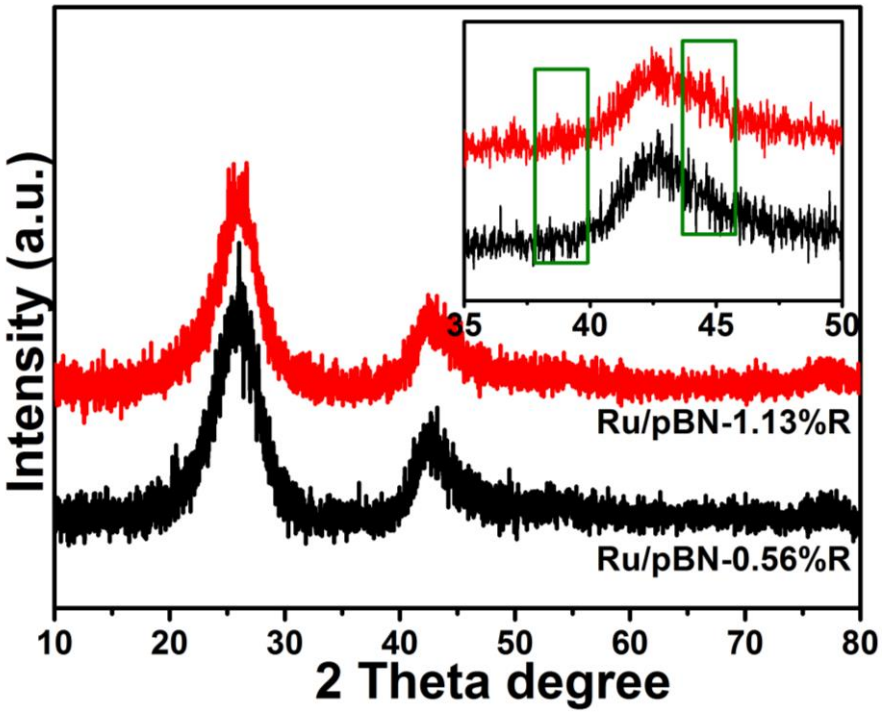

Figure S5. the XRD patterns of Ru/pBN-*x*R samples

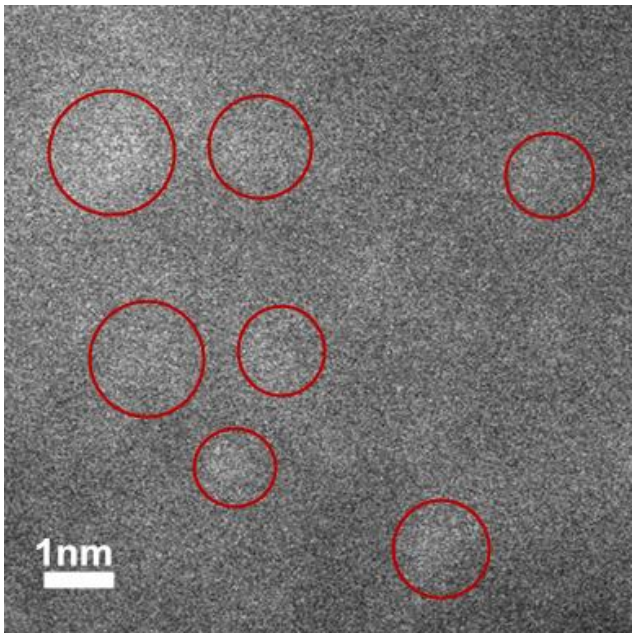

Figure S6. the HAADF-STEM image of Ru atoms in Ru/pBN-0.58%F (single Ru atoms labelled with red cricles).

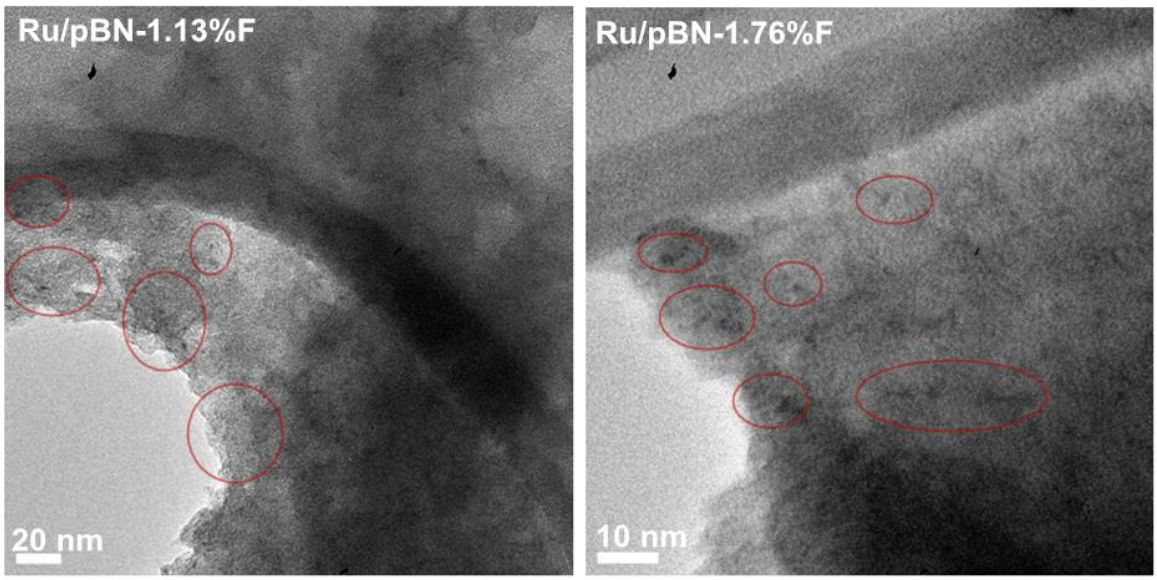

Figure S7. TEM images of Ru/pBN-1.13%F and -1.76%F.

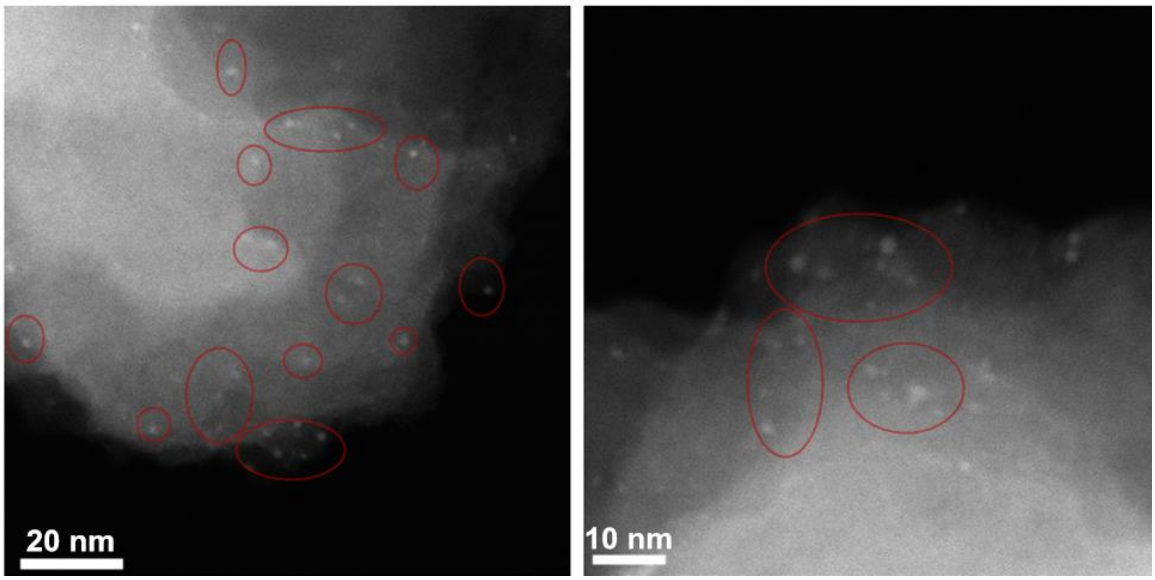

Figure S8. The Aberration-corrected HAADF-STEM images of Ru/pBN-0.56%R.

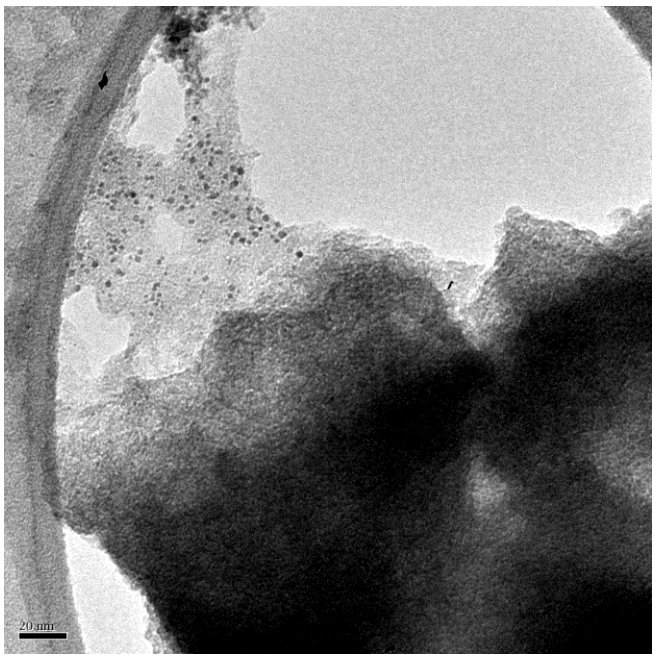

Figure S9. TEM image of Ru/pBN-1.13%R.

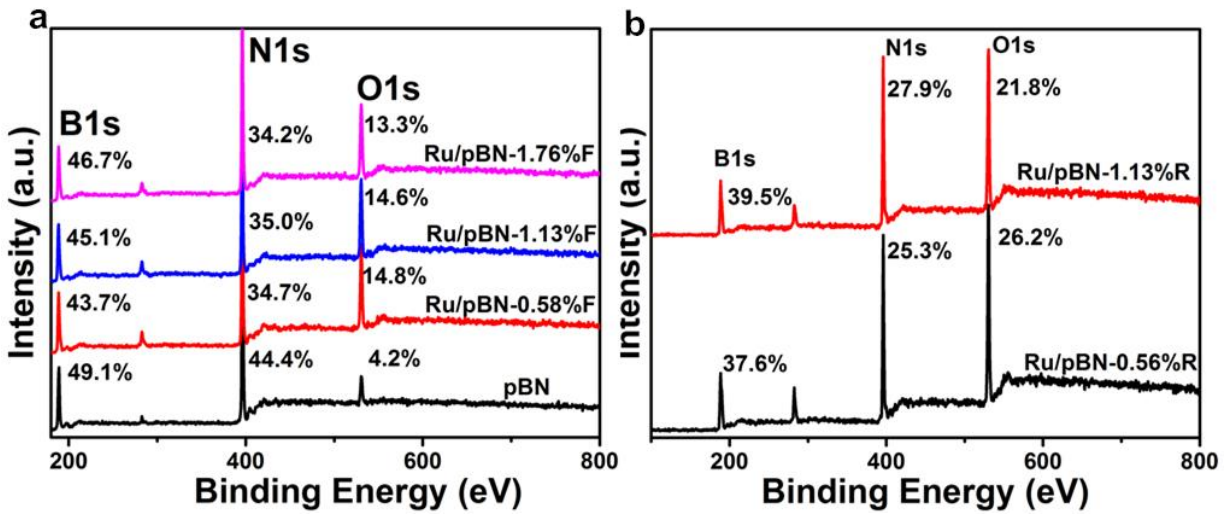

Figure S10. XPS survey spectra of Ru/pBN-*x*F (a) and Ru/pBN-*x*R (b) samples.

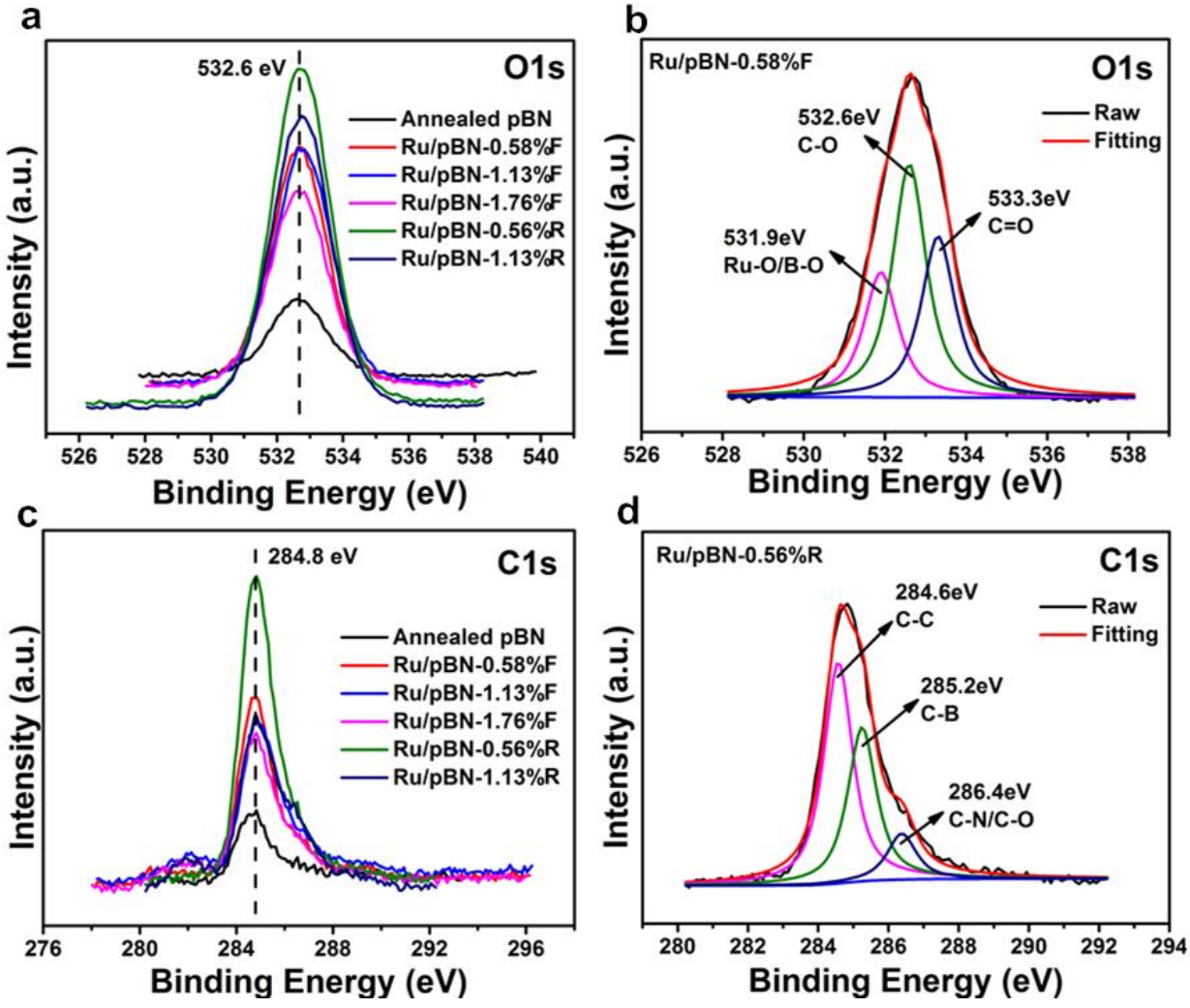

Figure S11. (a, c) The O1s and C1s spectra of annealed pBN and Ru/pBN samples. (b) The high-resolution of O1s in Ru/pBN-0.58%F. (d) The high-resolution of C1s in Ru/pBN-0.56%R.

When all samples were annealed, the binding energy of O is shifted from 531.2 eV (B-O) to 532.6 eV (**Figure S11a**) indicating the change of O species. According to the

fitting spectrum of O1s (**Figure S11b**), most of the O species can be attributed to C-O and C=O after annealing.[1, 2] Partial O is connected with B atoms, where O coordination with Ru is also one of O species.

According to C1s spectra **Figure S11c** and **d**, B atoms are easy bonded with C atoms as shown by the C-B peak.[3, 4] Due to the high C content in Ru/pBN-xR samples, this reduces the possibility of formation of B-N bonds. This explains the difference in the B/N ratios of Ru/pBN-xR samples (1.49, 1.42 for -0.56%R, -1.13%R, respectively) relative to the Ru/pBN-xF samples (1.26, 1.29, 1.37 for -0.58%F, -1.13%F, -1.76%F, respectively). The reason for different C impurities and O contents in Ru/pBN samples can be attributed to the catalytic effect of Ru on the removal of O species (most of them are bonded to C atoms) by forming CO_2 and H_2O during annealing progress. Compared to the Ru aggregation, the atomic Ru has higher catalytic activity so the Ru/pBN-xF samples have lower C, O contents (Figure S10).[5, 6]

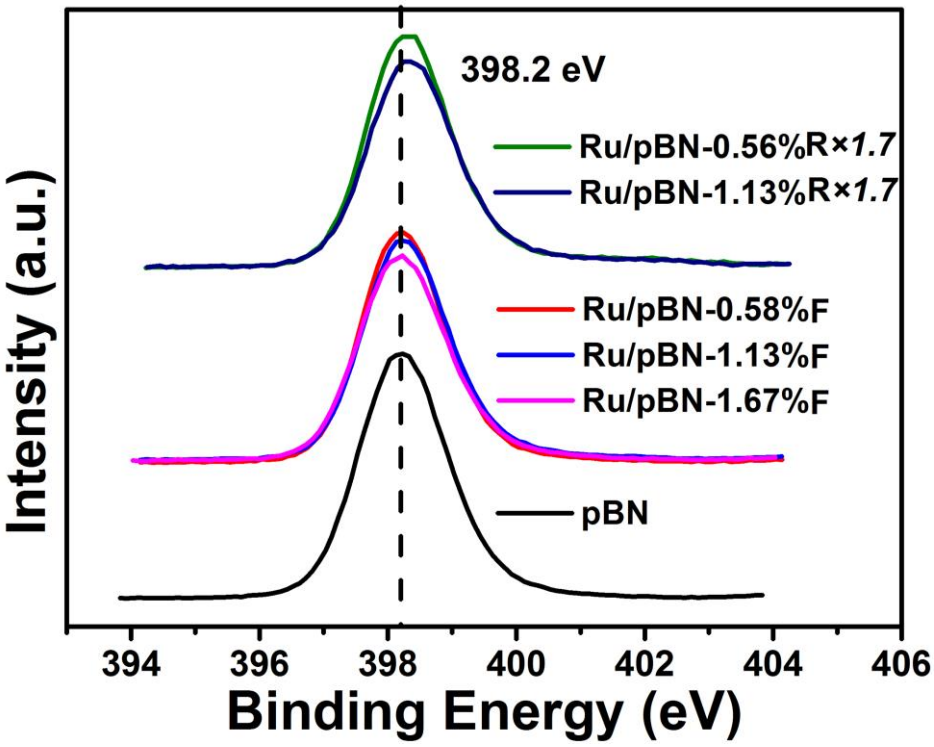

Figure S12. The N1s spectrum of Ru/pBN-*x*R, -*x*F samples

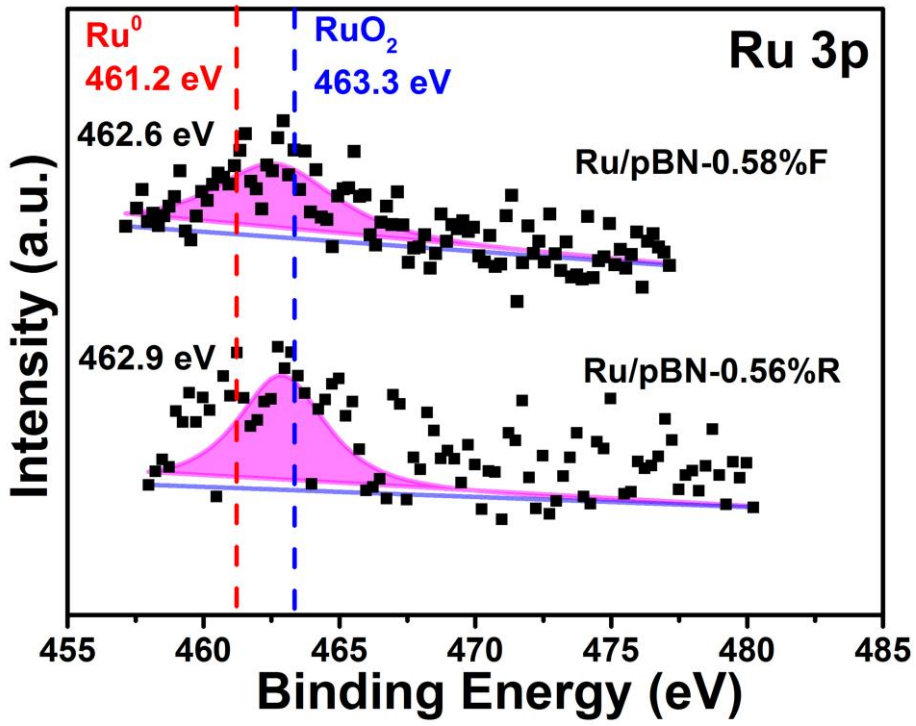

Figure S13. The high-resolution of Ru 3p in Ru/pBN-0.58%F and -0.56%R.

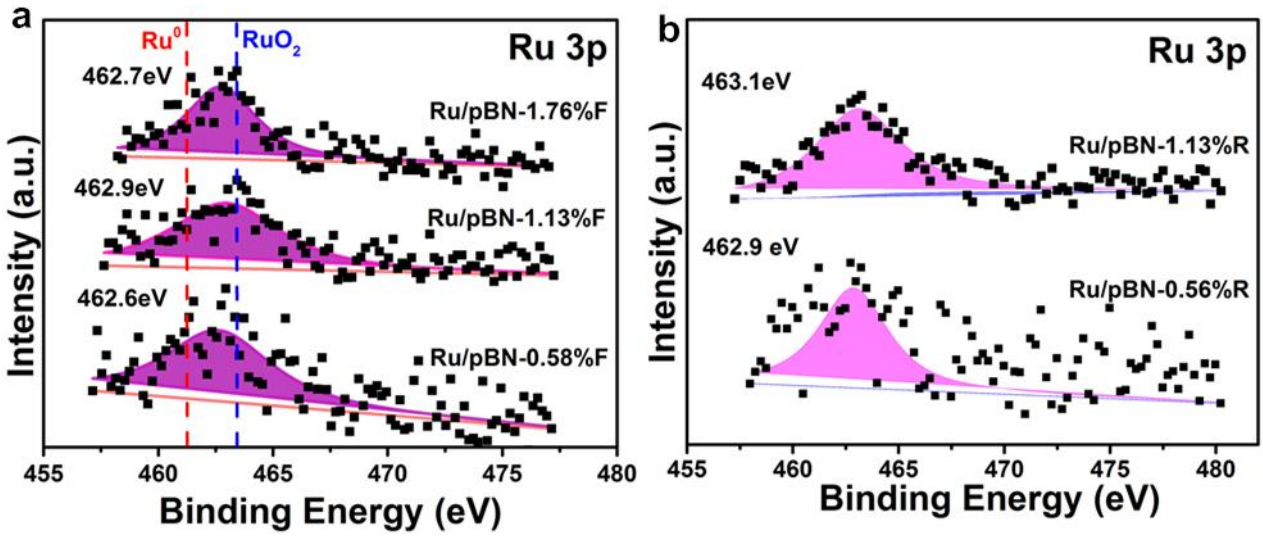

Figure S14. The high-resolution of Ru 3p in Ru/pBN-*x*F (a) and Ru/pBN-*x*R (b) samples.

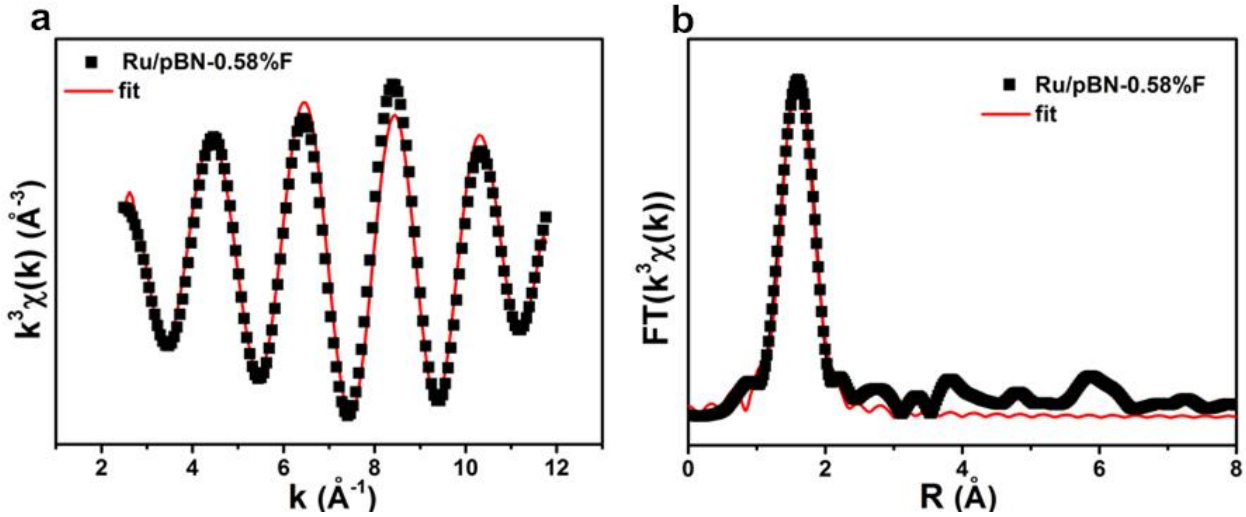

Figure S15. k^3-weighted EXAFS spectra for Ru/pBN-0.58%F in k-space (a) and the Fourier Transform in R space (b) with their corresponding fits.

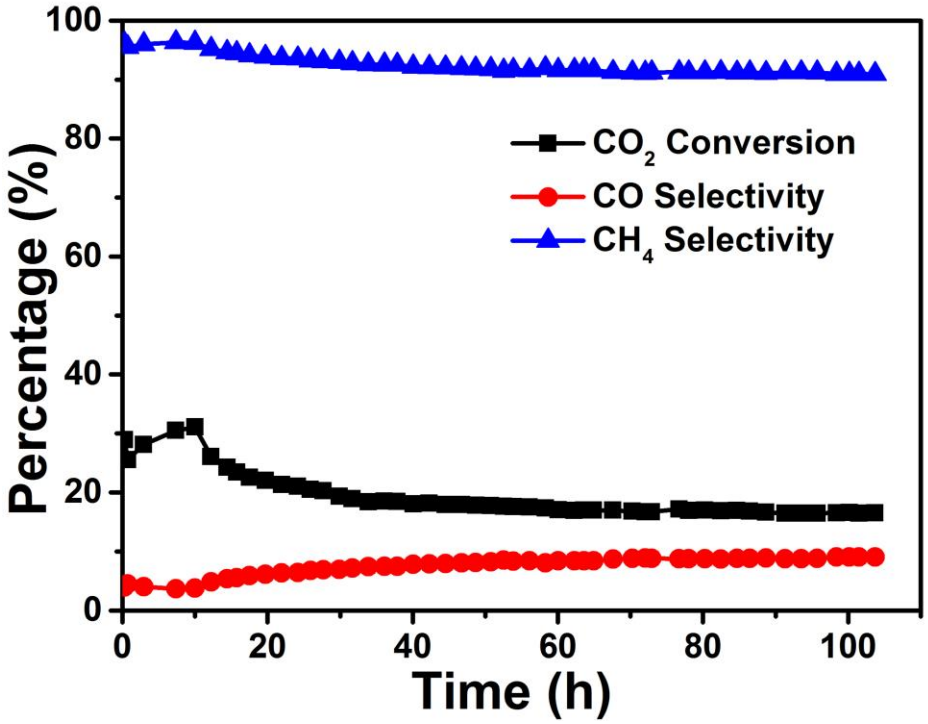

Figure S16. The catalytic stability of Ru/pBN-0.58%F for 110h. Reaction Conditions: 4:1 ratio of H_2:CO_2 with a 10% Ar internal standard, 10 bar pressure, 320 °C bed temperature, 18000 h^{-1} space velocity.

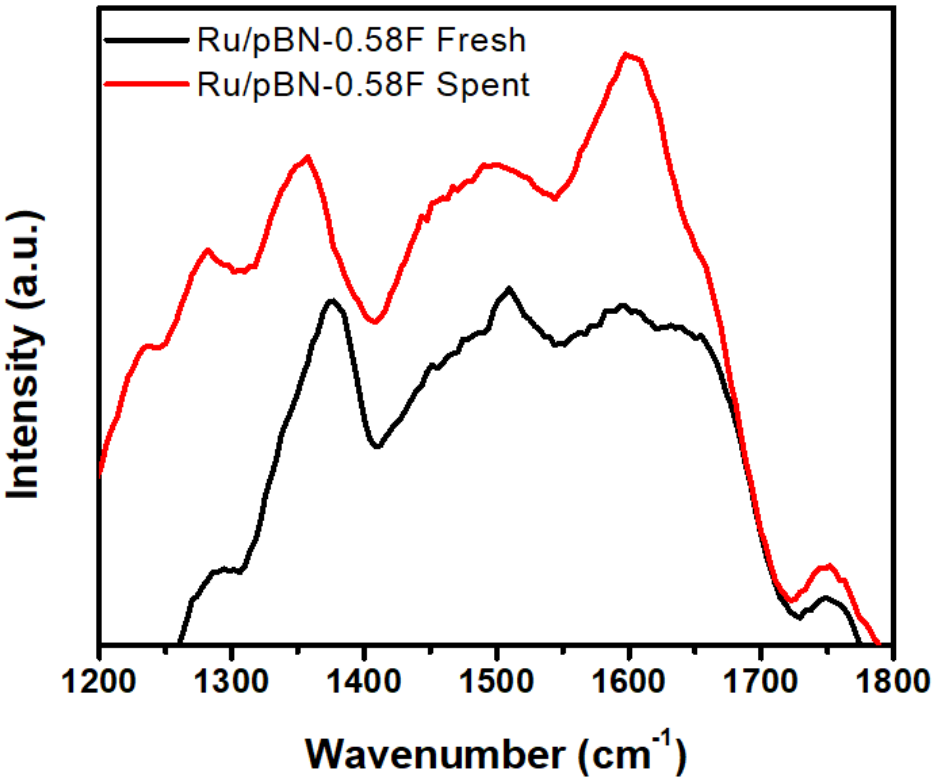

Figure S17. The Raman spectra of fresh and spent Ru/pBN-0.58%F for catalytic reaction.

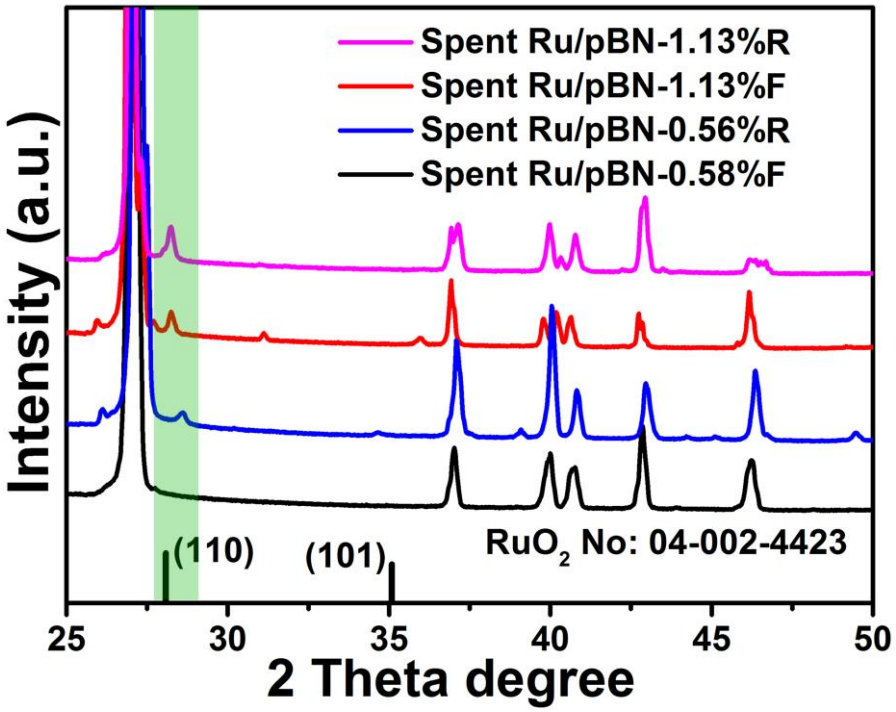

Figure S18. The XRD patterns of the spent Ru/pBN-*x*F and -*xR* samples.

Table S1. Ru K-edge EXAFS curve Fitting Parameters

Sample	Bond	Coordination number of N	Bond length	$\sigma^2(10^{-3}$ Å$^2)$
Ru/pBN-0.58%F	Ru-N/B	3.3	2.08	2.2
Ru foil	Ru-Ru*	12	2.68	3.3
RuO_2	Ru-O*	4	1.90	2.9
	Ru-O*	2	2.02	2.9

σ^2, Debye-Waller factor. Error bounds (accuracies) were estimated as N, ±10%; Bond length, ±1%; σ^2, ±10%. * is fixed coordination number according to the standard crystal structure.

Table S2. Comparison of catalytic activity for Ru/pBN-*x*F, Ru/pBN-*x*R, and selected CO_2 hydrogenation catalyst from literature

Catalyst	H_2:CO_2 Ratio	T. °C	P. MPa	Conv. (%)	CH_4 Sel. (%)	Reaction rate (mmol CO_2•gcat•s^{-1})	Ref.
Co/TiO_2 54 wt.%	4:1	341	1.0	75	99.5	0.03	7
Ru/TiO_2 0.8 wt.%	4:1	160	0.1	100	100	0.251	8
0.1%Ru/Al_2O_3	3:1	350	0.1	~2	~0	0.83	9
NGQDs/Al_2O_3	4:1	359	1.0	41.8	26.9	1.57	10
Ni/$Ce_xZr_{1-x}O_2$	4:1	350	0.1	79.7	99.3	0.66	11
Ru/pBN-0.58%F	4:1	350	1.0	28.7	93.5	1.86	This work
Ru/pBN-1.13%F	4:1	350	1.0	39.1	95.8	1.30	This work
Ru/pBN-1.76%F	4:1	350	1.0	40.1	96.4	0.85	This work
Ru/pBN-0.56%R	4:1	350	1.0	5.1	72.5	0.33	This work
Ru/pBN-1.13%R	4:1	350	1.0	6.5	76.8	0.22	This work

Simulation optimization in DFT

We considered the Eley-Rideal mechanism for simulating the RWGS mechanism for the hydrogenation of CO_2 to CH_4. The reaction steps considered in this work are given below.

$$CO_2(g) + 1/2\ H_2(g) \rightarrow\ ^*HOCO$$

$$^*HOCO + 1/2\ H_2(g) \rightarrow CO(g) + H_2O(g)$$

$$CO + 1/2\ H_2(g) \rightarrow\ ^*HCO$$

$$^*HCO + 1/2\ H_2(g) \rightarrow\ ^*H_2CO$$

$$^*H_2CO + 1/2\ H_2(g) \rightarrow\ ^*H_2COH$$

$$^*H_2COH + 1/2\ H_2(g) \rightarrow\ ^*CH_2 + H_2O(g)$$

$$^*CH_2 + 1/2\ H_2(g) \rightarrow\ ^*CH_3$$

$$^*CH_3 + 1/2\ H_2(g) \rightarrow CH_4(g)$$

The free energy of the products and reactants were calculated as $G = E_{DFT} + ZPE - TS + \Delta H$, where, E_{DFT} is the ground state energy calculated with DFT, ZPE is the zero-point energy, ΔH is the change in enthalpy and TS is the entropic contribution to free energy. The change in enthalpy from 0 to 298.15 K was taken from the CRC S5 Press Handbook of Chemistry and Physics, while enthalpy changes from 298.15 K to 623 K (350 ^{o}C) were taken from the NIST Chemistry WebBook and Computational Chemistry Comparison and Benchmark DataBase.

The doping energy is calculated as follows:

$$E_{doping} = E(vac + RuO_x) - E_{vac} - E_{Ru}(bulk) - E_{O_2}/2,$$

where, $E(vac + RuO_x)$ is energy of vacancy structure (B, N, BN, B_3N, BN_3) with RuO_x (x = 1 or 2) doping, E_{vac} is the energy of the vacancy structure. Whereas, $E_{Ru}(bulk)$ is energy of Ru atom in its bulk form and E_{O_2} is energy of O_2 molecule.

(1) Xu, J.-J.; Chang, Z.-W.; Wang, Y.; Liu, D.-P.; Zhang, Y.; Zhang, X.-B. Cathode Surface-Induced, Solvation-Mediated, Micrometer-Sized Li_2O_2 Cycling for Li-O_2 Batteries. *Adv. Mater*. **2016**, 28, 9620-9628.

(2) Ge, R.; Li, L.; Su, J.; Lin, Y.; Tian, Z.; Chen; L. Ultrafine Defective RuO2 Electrocatalyst Integrated on Carbon Cloth for Robust Water Oxidation in Acidic Media. *Adv. Energy Mater.* **2019**, 19013123.

(3) Ci, L.; Song, L.; Jin, C.; Jariwala, D.; Wu, D.; Li, Y.; Srivastava, A.; Wang, Z. F.; Storr, K.; Balicas, L.; Liu, F.; Ajayan, P. M. Atomic layers of hybridized boron nitride and graphene domains. *Nat. Mater.* **2010**, 9, 430-435.

(4) Fan, M.; Wu, J.; Yuan, J.; Deng, L.; Zhong, N.; He, L.; Cui, J.; Wang, Z.; Behera, S. K.; Zhang, C.; Lai, J.; Vajtai, R.; Deb, P.; Huang, Y.; Qian, J.; Yang, J.; Tour, J. M.; Lou, J.; Chu, C.-W.; Sun, D.; Ajayan, P. M. Doping nanoscale graphene domain improves magnetism in hexagonal boron nitride. *Adv. Mater.* **2019**, 1805778.

(5) Zhao, L.; Zhao, X.; Burke, L. T.; Bennett, J. C.; Dunlap, R. A.; Obrovac, M. N. Voronoi-Tessellated Graphite Produced by Low-Temperature Catalytic Graphitization from Renewable Resources. *ChemSusChem* **2017**, 10, 3409-3418.

(6) Chen, H.; Yang, Z.; Zhang, Z.; Chen, Z.; Chi, M.; Wang, S.; Fu, J.; Dai, S. Construction of a Nanoporous Highly Crystalline Hexagonal Boron Nitride from an Amorphous Precursor for Catalytic Dehydrogenation. *Angew. Chem. Int. Ed.* **2019**, 58, 10626-10630

(7) Jimenez, J.; Bird, A.; Santos Santiago, M.; Wen, C.; Lauterbach, J. Supported Cobalt Nanorod Catalysts for Carbon Dioxide Hydrogenation. *Energy Techno.* **2017**, 5, 884-891.

(8) Abe, T.; Tanizawa, M.; Watanabe, K.; Taguchi, A. CO_2 methanation property of Ru nanoparticle-loaded TiO_2 prepared by a polygonal barrel-sputtering method. *Energ. Environ. Sci.* **2009**, *2* (3), 315-315.

(9) Kwak, J. H.; Kovarik, L.; Szanyi, J. CO_2 Reduction on Supported Ru/Al_2O_3 Catalysts: Cluster Size Dependence of Product Selectivity. *ACS Catal.* **2013**, *3* (11), 2449-2455.

(10) Wu, J.; Wen, C.; Zou, X.; Jimenez, J.; Sun, J.; Xia, Y.; Fonseca Rodrigues, M.-T.; Vinod, S.; Zhong, J.; Chopra, N.; Odeh, I. N.; Ding, G.; Lauterbach, J.; Ajayan, P. M. Carbon Dioxide Hydrogenation over a Metal-Free Carbon-Based Catalyst. *ACS Catal.* **2017**, *7* (7), 4497-4503.

(11) Mikkelsen, M.; Jorgensen, M.; Krebs, F. C. The teraton challenge. A review of fixation and transformation of carbon dioxide. *Energ. Environ. Sci.* **2010**, *3* (1), 43-81.